45th AIAA Aerospace Sciences Meeting and Exhibit
8 - 11 January 2007, Reno, Nevada

AIAA 2007-856

Autonomous Maneuvering Entry Guidance with Ground-track Control

M. Sudhir* and Ashish Tewari†
Indian Institute of Technology, Kanpur 208016, India.

We demonstrate that a three-dimensional entry guidance with accurate ground-track control can be achieved using a combined strategy of proportional down-range (smart) maneuvering and linear quadratic (LQ) technique, thereby precluding the necessity of sophisticated nonlinear programming. It is also shown that heating rate and load-factor constraints can be met by a careful but simple selection of LQ gains. Two examples of entry trajectories are considered: a low-lift capsule with bank angle as the only control input and a reusable launch vehicle (RLV) with both lift-coefficient and bank angle as the control variables. Simulation results are compared with those of a planar guidance and a nonlinear guidance technique published previously. In the case of low-lift capsule, the controller is able to track the reference trajectory in presence of initial deviation from the nominal entry point, with small errors in the terminal states. Although the speed, flight path angle, and down-range accuracy are comparable to that of a planar guidance strategy, the present technique also demonstrates an accurate cross-range control not possible with a planar strategy. Results for a RLV vehicle indicate the effectiveness of the control law for large initial offsets from a reference trajectory. It is shown that smart maneuvering produces a superior performance than that of a nonlinear tracking control derived using feedback linearization. The method can handle much larger deviations in the entry conditions than those published previously, and has the important advantage of a relatively simple implementation in a realistic entry scenario. Furthermore, the LQ technique can take advantage of the good robustness properties of a linear Kalman filter based upon the measurement of longitude, latitude, and speed, wherein little deterioration is observed in the closed-loop performance.

Nomenclature

$A(t)$	= state dynamics matrix.
$B(t)$	= state input coefficient matrix.
C_D	= drag coefficient.
C_F	= skin friction coefficient.
C_L	= lift coefficient.
D	= drag force.
$E[.]$	= expected value operator.
e_o	= estimated error of the reduced-order observer.
g	= acceleration due to gravity.
G, H, M	= co-efficient matrices of reduced-order observer.
h	= altitude.
I_{nxn}	= identity matrix of order n.
J	= objective function.
$K(t)$	= feedback LQ gain matrix.
$K_o(t)$	= observer gain matrix.
k_1, k_2	= constant feedback gains for down-range maneuvering.
L	= lift force.

* Doctoral Student, Department of Aerospace Engineering. Member, AIAA. E-mail: msudhir@iitk.ac.in.
† Associate Professor, Department of Aerospace Engineering. Senior Member, AIAA. E-mail: ashtew@iitk.ac.in

m = mass.
n = total load-factor.
$P(t)$ = solution of the algebraic Riccati equation.
Q = state weighting matrix.
Q_h = heating rate.
q = dynamic pressure.
R = input weighting matrix.
R_C = combined range ($R_c = \sqrt{X^2 + Y^2}$).
R_E = radius of the Earth.
R_e = optimal covariance matrix.
r = distance from the Earth's center.
S = reference area.
S_w = total wetted area.
t = time.
t_d = time of down-range maneuvering.
$u(t)$ = input vector.
V = relative speed.
$v(t)$ = process noise.
X = down-range.
$x(t)$ = state vector.
$x_1(t)$ = measured state vector.
$x_{o2}(t)$ = estimated state vector.
Y = cross-range.
$Z_k(t)$ = power spectral density matrix of $z_k(t)$.
$z(t)$ = reduced order observer state vector.
$z_k(t)$ = measurement noise.
α = angle of attack.
γ = flight path angle.
$\delta(.)$ = deviation from nominal trajectory.
θ = longitude.
μ = gravitational constant.
ρ = atmospheric density.
σ = bank angle.
φ = latitude.
ψ = heading angle.
ω = planet's angular velocity.

Subscripts

com = commanded variables.
f = terminal values.
max = maximum allowable values.
o = observer.
s = surface of planet.
r = nominal/reference variables.

Overdot

time-derivative.

I. Introduction

A primary focus in entry technology and development of a reusable launch vehicle (RLV) is entry guidance and control. In the past, several distinct approaches[1] have been considered for entry guidance, which can be grouped into two general categories: (a) path-predicting, where the controller uses a near real-time prediction to generate the trajectory and the required controls in flight, and (b) path-following, wherein the controller tracks a pre-determined reference trajectory.

The path-predicting methods have the disadvantage of large on-board computer requirements, and a limited capability of handling off-design conditions. Such methods can be sub-classified into approximate closed-form prediction and fast-time prediction. The problem of determining a feasible entry trajectory, that meets the constraints

of heating rate, axial and transverse load-factors results in an optimal control input which is inherently nonlinear, and requires geometric, nonlinear programming methods. In order to avoid solving the complete optimal guidance problem in real-time, a practical alternative is closed-form, analytical solution based on approximate dynamics[2-4]. However simple closed-form solutions usually do not have the flexibility to handle markedly off-design conditions. The fast-time prediction is based upon repetitive solution of the equations of motion in real-time, in order to determine possible future trajectories. This method has the ability to handle any possible flight condition, but again requires large on-board computing facilities.

In contrast to path-predicting techniques, a path-following guidance about nominal trajectories provides a simple guidance method that can be designed to accommodate off-design entry conditions. Path-following guidance techniques involve guidance about a nominal trajectory, where the state variables along the nominal path are pre-computed and stored on-board. The variations in the measured variables from the stored values are used in guidance either to track the nominal trajectory (path control) or to establish a new trajectory in order to reach the destination (terminal control). The desired nominal trajectories are selected and stored apriori by solving the two-point, boundary-value problem (TPBVP). For the three dimensional Apollo-type re-entry problem, Williamson and Tapley[5] use a successive linear solution, Stoer and Bulirsch[6] employ a multiple shooting method, Yeo and singh[7] adopt a quasi-linearization approach for a problem with control bounds, whereas Trent et al.[8] propose a modified simple shooting method for a planar problem.

The path-following guidance methods[9-17] can be classified as either linear or nonlinear based upon the kind of trajectory control used. The guidance can be of path control with fixed feedback gains, terminal control having influence coefficients (closed-form, bang-bang, etc.), and optimal feedback gains. A closed-form solution of the equation of motion is used in the U.S. space shuttle guidance,[9, 10] where the down-range is controlled by issuing bank angle magnitude commands to track a drag acceleration profile. The profile is also re-planned onboard during entry to correct for tracking errors and to nullify the predicted down-range error. The cross-range is controlled by issuing bank reversal commands to keep the heading error within certain bounds. Virgilio et al.[11] apply linear optimal (LQ) guidance to ballistic type vehicles. Both Refs.11 and 12 address the determination of the weighting matrices required for LQ regulator design. Archer[13] formulates the linear control problem with a trajectory variable instead of time. Roenneke and Cornwell[14] design a tracking controller for a low-lift re-entry vehicle, where the reference trajectory is defined by altitude, velocity, and flight-path angle. Position and heading angles are not included in the controller design. Roenneke and Markl[15] schedule the drag profile as functions of energy for the entire trajectory for accurate range prediction, and the reference profile is parameterized by cubic splines. For trajectory control, they employ a linear feedback control law whose gains are scheduled to vary with the energy. Lu[16] use linear receding-horizon control law for the X-33 vehicle, while Shen and Lu[17] employ an LQ based proportional-integral (PI) control law for lateral entry guidance. They have found that, the cross-range is a more suitable parameter than the heading error for lateral guidance.

A nonlinear control law based on the feedback linearization method is compared with shuttle trajectory control law in Ref. 18. Cavallo and Ferrara[19] propose a control strategy which is based on the (LQ) design technique and on the variable structure systems (VSS) mathematical machinery applied to assured crew return vehicle (ACRV). They employ a sliding-mode controller in conjunction with the LQ technique to meet the ground-track requirements. Several authors[20-22] have proposed and evaluated variations to the shuttle entry guidance for medium to high L/D vehicles. All of these retained the basic assumption of the shuttle drag planning. Lu et al.[20, 21] however, included a final pre-terminal area energy management (pre-TAEM) phase to increase the capability of meeting the TAEM conditions.

This paper presents the trajectory control of lifting re-entry vehicles using a combined strategy of down-range maneuvering and an LQ design technique. The present autonomous strategy is to be contrasted with previously published techniques wherein a terminal control for the slow dynamics given by the longitude, latitude and heading angles is carried out independently of the fast dynamics given by altitude, velocity and flight-path angle. Such an approach-based upon tracking only a few variables at a time – is unable to meet the ground-track accurately, especially in the presence of moderate deviations from the nominal entry point. Our approach is based upon a simultaneously penalty on all the state variables applied continuously from entry to TAEM, resulting in an accurate ground-track control. In the presence of down-range deviations, a “smart” maneuvering algorithm is devised such that either a turn-back or a pull-up is carried out depending upon whether the vehicle has over-shot or under-shot the nominal entry point. The smart maneuvering is carried out with proportional banking (or lifting) for a pre-determined duration.

The new strategy is applied to two vehicles: a low-lift capsule where the bank angle is the only control input, and another an RLV, which requires modulation of both lift-coefficient and bank-angle. The results compare favorably with those obtained from a nonlinear geometric tracking law derived using feedback linearization[22].

Results for entry deviations much larger than those previously published show the efficacy and simplicity of the scheme. Thus it is demonstrated that a well designed, simple control concept is sufficient for re-entry trajectory control, even in the presence of large deviations in entry conditions, without exceeding the maximum allowable aerothermal loads. Furthermore, it is shown that a linear Kalman filter based upon the measurement of longitude, latitude, and speed, results in an accurate tracking of all state variables, including the ground-track.

II. Entry Dynamics

The translational equations of motion of an unpowered re-entry vehicle of mass, *m,* flying inside the atmosphere of the spherical, rotating planet are used to simulate the guiding controller's performance. The state vector is chosen to comprise the standard planet fixed variables, $x(t) = (r,\theta,\varphi,V,\gamma,\psi)^{\mathrm{T}}$, while control vector is $u(t) = (\sigma,C_L)^{\mathrm{T}}$. The kinematic equations of motion can be written as follows[23]:

$$\dot{r} = V\sin\gamma \tag{1}$$

$$\dot{\theta} = \frac{V\cos\gamma\cos\psi}{r\cos\phi} \tag{2}$$

$$\dot{\phi} = \frac{V\cos\gamma\sin\psi}{r} \tag{3}$$

whereas the dynamical equations of motion are

$$\dot{V} = -\frac{D}{m} - g\sin\gamma + \omega^2 r\cos\phi(\sin\gamma\cos\phi - \cos\gamma\sin\phi\sin\psi) \tag{4}$$

$$\begin{aligned}\dot{\gamma} = {} & \frac{L\cos\sigma}{mV} - \left(\frac{g}{V} - \frac{V}{r}\right)\cos\gamma + 2\omega\cos\phi\cos\psi \\ & + \frac{\omega^2 r\cos\phi(\cos\gamma\cos\phi + \sin\gamma\sin\phi\sin\psi)}{V}\end{aligned} \tag{5}$$

$$\begin{aligned}\dot{\psi} = {} & \frac{L\sin\sigma}{mV\cos\gamma} - \frac{V\cos\gamma\cos\psi\tan\phi}{r} \\ & + 2\omega(\tan\gamma\cos\phi\sin\psi - \sin\phi) - \frac{\omega^2 r\sin\phi\cos\phi\cos\psi}{V\cos\gamma}\end{aligned} \tag{6}$$

The aerodynamic lift and drag have the following standard form based upon non-dimensional coefficients:

$$L = \frac{1}{2}\rho V^2 S C_L \tag{7}$$

$$D = \frac{1}{2}\rho V^2 S C_D \tag{8}$$

The Newtonian gravitational law $g = \mu / r^2$ is employed for a spherical planet, while the stagnation point (maximum) heating rate, the load-factor, and dynamic pressure are given by

$$Q_h = \frac{1}{4} C_F \rho S_W V^3 \tag{9}$$

$$n = \sqrt{\frac{L^2 + D^2}{mg_s}} \tag{10}$$

$$q = \frac{1}{2} \rho V^2 \tag{11}$$

III. Trajectory Control

The design of LQ guidance laws requires a linearization of Eqs. (1) – (6) about the nominal trajectory. A perturbed state $\delta x = (\delta r, \delta\theta, \delta\varphi, \delta V, \delta\gamma, \delta\psi)^T$ is defined such that $x = x_r + \delta x$, and correspondingly, a perturbed control is given by $\delta u = \delta\sigma$ such that $\delta u = u - u_r$. Here δC_L=0, as the LQ guidance law is used mainly to bring the cross-range and velocity deviations to zero at the terminal time. For small perturbations, Eqs. (1) – (6) can be linearized into

$$\dot{\delta x} = A(t)\delta x + B(t)\delta u \tag{12}$$

The time-varying linearized system's coefficient matrices *A(t)* and *B(t)* are obtained at discrete time intervals from the reference trajectory. The LQ objective function[24] is given by

$$J(t, t_f) = \int_t^{t_f} [\delta x^T(\tau) Q \delta x(\tau) + \delta u^T(\tau) R \delta u(\tau)] d\tau \tag{13}$$

where Q is positive semi-definite matrix and R>0 are state weighting and input weighting factors, respectively. Minimization of J in Eq. (13) as $t_f \to \infty$, results in an algebraic Riccati equation given by

$$PA - PBR^{-1}B^T P + Q + A^T P = 0 \tag{14}$$

Eq. (14) is solved for the constant *P(t),* at each time instant, *t*, in order to get the optimal gain matrix. The feedback gains are given by

$$K(t) = -R^{-1}B^T(t)P(t) \tag{15}$$

and the full-state feedback control-law is

$$\delta u(t) = -K(t)\delta x(t) \tag{16}$$

The weighting factors Q and R are chosen such that, the terminal errors in the important state variables are small, and the aerothermal load limits are never exceeded at any point in the trajectory.

In the design of a reduced-order Kalman filter, the state and the output equations are

$$\delta \dot{x}(t) = A(t)\delta x(t) + B(t)\delta u(t) + F(t)v(t) \tag{17}$$

$$\delta y(t) = C(t)\delta x(t) + D(t)\delta u(t) + z_k(t) \tag{18}$$

The state-vector of the plant, $\delta x(t)$, is partitioned into measured state variables, $\delta x_1(t)$, and the estimated state variables, $\delta x_2(t)$.

$$\delta x(t) = \begin{bmatrix} \delta x_1(t) \\ \delta x_{o2}(t) \end{bmatrix} \tag{19}$$

The estimated state-vector is given by

$$\delta x_{o2}(t) = K_o \delta y(t) + z(t) \tag{20}$$

where, $z(t)$ is an observer state vector satisfying the following state-equation

$$\dot{z}(t) = Mz(t) + Hu(t) + Gy(t) \tag{21}$$

The optimal Kalman filter gain is thus given by[24]

$$K_o(t) = R_e(t,t)C^T(t)Z_k^{-1}(t) \tag{22}$$

where

$$R_e(t,t) = E[e_o(t)e_o^T(t)] \tag{23}$$

is the optimal covariance matrix obtained from the solution of the associated Riccati equation[24], Z_k is the power spectral density of measurement noise $z_{k,}$ and the estimated error e_o is given by

$$e_o(t) = \delta x_2(t) - \delta x_{o2}(t) \tag{24}$$

A down-range (smart) maneuvering algorithm is used to minimize the final ground-track error resulting from perturbations in down-range. The algorithm consists of separate proportional control laws for either positive, or negative perturbations in the down-range:

$$u = u_r + \delta u_{com} \tag{25}$$

where,

$$\delta u_{com} = \begin{Bmatrix} \delta\sigma_{com} \\ \delta C_{L_{com}} \end{Bmatrix} = \begin{Bmatrix} \begin{pmatrix} k_1 \delta R_c \\ 0 \end{pmatrix}, \delta X > 0, t \le t_d \\ \begin{pmatrix} 0 \\ k_2 \delta R_c \end{pmatrix}, \delta X < 0, t \le t_d \\ \begin{pmatrix} -K\delta x \\ 0 \end{pmatrix}, t > t_d \end{Bmatrix} \tag{26}$$

k_1 and k_2 are constant gains, δR_c is the combined range error given by

$$\delta R_c = R_E \sqrt{\delta X^2 + \delta Y^2} \tag{27}$$

and t_d is the duration of smart maneuvering that is pre-determined from the down-range deviation at re-entry. The smart maneuvering is carried out for $0 \le t \le t_d$, while the LQ control law is applied for $t > t_d$. In the case of positive down-range perturbations, the lift-coefficient is unchanged from the nominal value while the bank angle is

modulated to execute a horizontal turn back towards the nominal trajectory. For negative down-range perturbations, the bank angle is unchanged from the nominal value while the lift co-efficient is increased in order to pull-up the vehicle towards the nominal trajectory.

Table 1. Nominal and off-nominal entry conditions for Model I and II

State variable	Model I			Model II		
	Nominal	Case A	Case B	Nominal	Case I	CaseII
x	x_r	$x_r+\delta x$	$x_r-\delta x$	x_r	δx	δx
h (km)	120	120	120	60.96	$\pm$ 0.3048	0.0
θ, deg.	0.0	0.0	0.0	0.0	$\pm$ 0.1	$\pm$ 0.45
φ, deg.	0.0	0.0	0.0	0.0	$\pm$ 0.1	0.0
V, m/s	7440.3	7422.5	7458.3	5181.6	0.0	0.0
γ, deg.	-2.97	-3.30	-2.60	0.0	0.0	0.0
ψ, deg.	0.0	0.0	0.0	0.0	0.0	0.0

Table 2. Weighting matrices for Model I for Case B

Case	*Q*	*R*
1	I_{6x6}	1.00 x10^{10}
2	I_{6x6}	2.00 x10^{10}
3	I_{6x6}	3.00 x10^{10}
4	I_{6x6}	2.10 x10^{10}
5	I_{6x6}	2.20 x10^{10}
6	I_{6x6}	2.30 x10^{10}
7	I_{6x6}	2.40 x10^{10}
8	diag [1 2.30 x10^{10} 2.30 x10^{10} 1 1 1]	2.30 x10^{10}
9	diag [1 2.30 x10^{11} 2.30 x10^{11} 1 1 1]	2.30 x10^{10}
10	diag [1 2.20 x10^{11} 2.20 x10^{11} 1 1 1]	2.20 x10^{10}
11	diag [1 2.10 x10^{11} 2.10 x10^{11} 1 1 1]	2.10 x10^{10}
12	diag [1 2.00 x10^{11} 2.00 x10^{11} 1 1 1]	2.00 x10^{10}
13	diag [1 1.90 x10^{11} 1.90 x10^{11} 1 1 1]	1.90 x10^{10}
14	diag [1 1.80 x10^{11} 1.80 x10^{11} 1 1 1]	1.80 x10^{10}
15	diag [1 1.70 x10^{11} 1.70 x10^{11} 1 1 1]	1.70 x10^{10}
16	diag [1 1.90 x10^{11} 1.90 x10^{11} 1 1 1]	1.80 x10^{10}
17	diag [1 1.70 x10^{11}1 1.70 x10^{11} 1 1 1]	1.80 x10^{10}
18	diag [1 1.60 x10^{11} 1.60 x10^{11} 1 1 1]	1.80 x10^{10}
19	diag [1 1.70 x10^{11} 1.70 x10^{11} 1 1 10]	1.80 x10^{10}
20	diag [1 1.70 x10^{11} 1.70 x10^{11} 1 2 10]	1.80 x10^{10}
21	diag [1 1.70 x10^{11} 1.70 x10^{11} 1 3 15]	1.80 x10^{10}
22	diag [1 1.650 x10^{11} 1.650 x10^{11} 1 3 10]	1.80 x10^{10}
23	diag [1 0 0 0.1 100 0]	1.00 x10^{09}

IV. Simulation Results

To demonstrate the trajectory control concept two vehicle models are chosen, an entry capsule with low-lift (Model I), and an RLV with adequate lifting capability (Model II). The U.S standard atmosphere 1976 is used to model the Earth's atmosphere, while the integration of nonlinear equations of motion is performed using a variable

step, fourth-order Runge-Kutta method. The effect of off-nominal entry conditions on the relative speed and flight path angle are considered in Model I, whereas for Model II, perturbations in initial longitude, latitude and altitude are also considered.

Model I

Model I represents a small re-entry capsule[14], which has a sphere-cone configuration with a base diameter 0.5 m, height 0.8 m, and mass 80 kg. To provide aerodynamic lift, one side of the cone is flattened, resulting in a constant supersonic lift-to-drag ratio of 0.52. The capsule's bank angle can be changed by a moving mass.

For the following simulation, reference trajectory with constant 45 deg. bank angle is chosen. The off-nominal entry conditions are due to ±10% deviation in de-orbit impulse[14], which produces offsets in the relative speed (δV), and flight path angle ($\delta\gamma$) as shown in Table 1.

The choice of weighting matrices (Q, R) is the crucial part in the design of LQ controller. The pair (Q,R) is chosen based upon the simulated terminal errors in the states, control input limitations, and aero-thermal loads. In the calculation of maximum heating rate for the Model I, we assume $C_F = 4C_D$. Table 2 lists the various cases tried in the selection of weighting matrices, while Table 3 presents the resulting terminal errors in each case. Clearly, Case 20 has the smallest terminal state error, of which the ground-track error is very small (0.2066 km). When aero-thermal loads are considered in Table 4, Case 2 has the smallest heating rate among all cases. By increasing the bank angle, the aero-thermal loads increases. Hence, there is a trade-off between the terminal state errors and aero-thermal loads.

Table 3. Terminal state errors for Model I for Case B

Case	Terminal ground-track error (δR_c) (km)	Terminal altitude error (δh) (km)	Terminal velocity error (δV) (m/s)	Terminal flight- path angle error ($\delta\gamma$) (deg.)	Terminal heading angle error ($\delta\psi$) (deg.)
1	30.9397	-0.0135	-0.2929	0.0001	5.0577
2	16.5049	0.0228	0.1387	-0.0007	-0.2642
3	26.2114	0.0184	0.1687	0.0274	-1.6415
4	14.9712	0.0050	0.0315	-0.0183	1.4490
5	14.6089	0.0305	0.2919	0.0201	-1.0498
6	14.2912	0.0194	0.1866	0.0096	-0.2257
7	14.5152	0.0390	0.2983	0.0171	-1.5305
8	11.5747	-0.0049	-0.0809	0.2422	-8.6021
9	9.6908	0.1379	-0.2115	4.1167	108.1844
10	7.0877	0.0098	0.2625	-0.2843	4.8072
11	5.7877	-0.0002	0.0552	0.0148	0.7297
12	3.4374	0.0044	0.1475	-0.3079	1.5196
13	1.1186	0.0180	0.0201	0.3563	1.3922
14	0.8708	0.0066	0.0134	0.1292	-4.5346
15	1.7639	0.0017	-0.0281	0.2302	8.2360
16	1.1678	-0.0003	-0.0251	0.0429	-0.0504
17	0.2622	0.0040	0.0378	-0.0129	-8.9254
18	0.8840	0.0005	0.1464	-0.1711	9.0986
19	0.7992	0.0279	-0.2492	1.2256	0.8310
20	0.2066	0.0007	-0.0083	0.1010	1.1323
21	0.8173	0.0126	0.1041	-0.0580	-0.2104
22	0.5508	0.0258	0.2746	-0.3039	-0.5335
23	182.4179	-0.2459	2.0808	0.8442	-25.1387

We shall consider two alternative strategies: planar guidance (similar to that of Ref. 14) without considering ground-track, and nonplanar guidance, wherein deviations in ground-track are penalized in addition to the other state variables. Note that nonplanar guidance is covered in Case 1-22 of Tables 2 and 3, while the planar strategy is

limited to Case 23. Figure 1 shows the time history of altitude, velocity, and flight-path angle due to a +10% (Case A) and -10% (Case B) deviations in de-orbit impulse with the planar guidance law. Although the planar strategy successfully tracks the profile of Ref. 14, it fails to meet the nominal ground-track (not considered in Ref. 14), resulting in unacceptable terminal range deviation. The bank angle profile and the aerothermal loads for perturbed entry with the planar guidance are compared with those of the nominal trajectory in Fig. 2.

Table 4. Maximum control input and aero-thermal loads for Model I for Case B

Case	Maximum bank angle, σ (deg.)	Maximum dynamic pressure, q (N/m^2)	Maximum Heating rate, Q_h (W/ m^2)	Maximum load factor, n (g)
1	78.5915	7.43 x10^3	7.91 x10^6	3.07
2	69.8871	6.62 x10^3	6.69 x10^6	2.97
3	64.4860	7.06 x10^3	7.25 x10^6	3.06
4	69.2427	6.61 x10^3	6.71 x10^6	2.91
5	68.6029	6.68 x10^3	6.77 x10^6	2.90
6	67.9788	6.68 x10^3	6.78 x10^6	2.91
7	67.4069	6.72 x10^3	6.84 x10^6	2.91
8	68.4513	7.36 x10^3	7.39 x10^6	3.15
9	146.5194	8.70 x10^3	8.74 x10^6	3.69
10	77.5533	8.72 x10^3	8.77 x10^6	3.70
11	69.8919	8.74 x10^3	8.81 x10^6	3.72
12	70.3848	8.80 x10^3	8.87 x10^6	3.74
13	70.8409	8.83 x10^3	8.92 x10^6	3.76
14	71.4197	8.89 x10^3	8.95 x10^6	3.78
15	71.8214	8.97 x10^3	9.02 x10^6	3.81
16	71.2144	8.92 x10^3	8.98 x10^6	3.80
17	71.1761	8.84 x10^3	8.88 x10^6	3.76
18	71.0942	8.79 x10^3	8.84 x10^6	3.74
19	76.2617	8.84 x10^3	8.91 x10^6	3.76
20	71.1782	8.86 x10^3	8.93 x10^6	3.77
21	71.1807	8.90 x10^3	8.94 x10^6	3.77
22	71.1090	8.83 x10^3	8.88 x10^6	3.76
23	103.6322	7.93 x10^3	9.73 x10^6	3.53

The closed-loop trajectory obtained by the nonplanar approach of Case 20 (Table 3) is plotted in Fig. 3, demonstrating a convergence to the desired terminal state, including ground-track. The largest bank angle for nonplanar guidance (Fig.4) is smaller than that required for planar guidance (Fig.2). As a result, the peak heating rate is smaller for the nonplanar method, as shown in Fig.4, although a slight increase in the load-factor is observed, compared to that of planar method. Thus the nonplanar guidance law outperforms the planar one in terms of ground-track error, bank angle input and aerothermal loads. Hence, there is no need for separate dedicated ground-track control claimed in Ref.14. The down-range maneuvering (Eq. 26) is not necessary in this case. The next example is more interesting, because it includes down-range deviation at entry.

Model II

Model II represents an RLV[22] corresponding to the SX-2 vehicle of erstwhile McDonnell Douglas Corp., with a maximum lift-to-drag ratio of 1.6. A polynomial fit of the aerodynamic data for $C_L(\alpha)$ and $C_D(\alpha)$ over the range $5 < \alpha < 25$ deg., including the effects of flap deflections for trimming the vehicle, is given by[22]

$$C_L(\alpha) = 2.5457\,\alpha - 0.0448 \tag{28}$$

$$C_D(\alpha) = 3.7677\,\alpha^2 - 0.1427\,\alpha + 0.197 \tag{29}$$

The mass during descent is constant at 37335 kg, and S=65.9 m^2. Since in this case $\delta\psi$=0, we have $\delta X = r\delta\theta$, consequently the duration of smart maneuvering, t_d, depends solely on the initial perturbation in the longitude $\delta\theta$. An

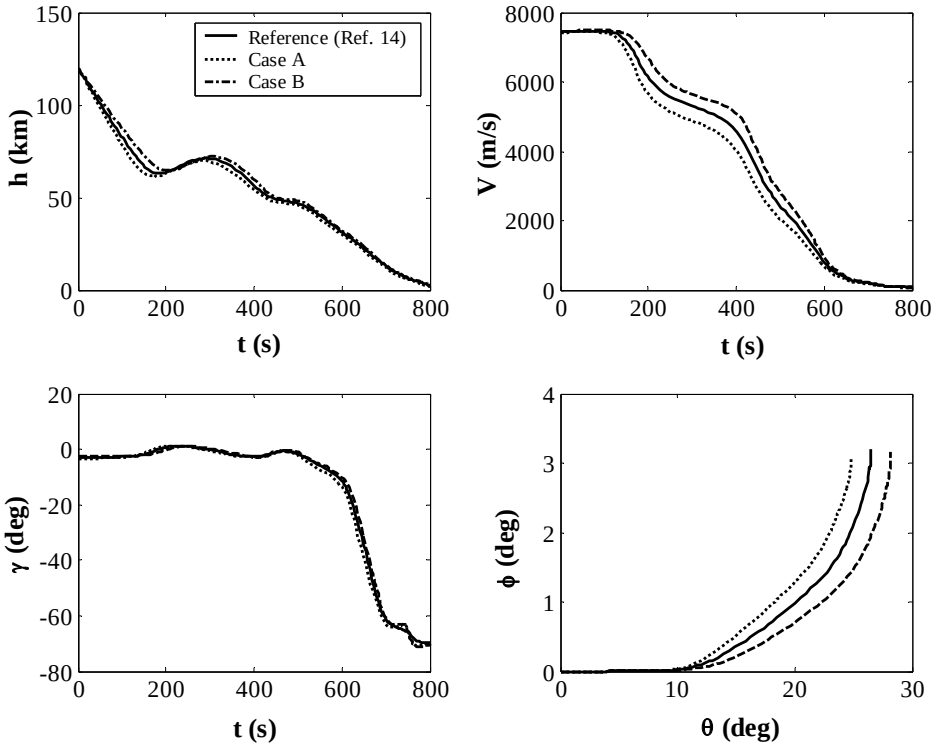

Figure 1. Trajectory profiles and ground-track for Model I using Controller A

empirical relation for t_d in terms of initial perturbation in longitude has been derived in the range of $0.05 \le |\delta\theta| \le 0.45$ deg. to be the following:

$\underline{\delta\theta > 0.05}$:

$$t_d = -24615\delta\theta^5 + 36946\delta\theta^4 - 21862\delta\theta^3 + 6530.9\delta\theta^2 - 1035.7\delta\theta + 87.917 \quad (30)$$

$\underline{\delta\theta < -0.05}$:

$$t_d = 303.03\delta\theta^4 + 252.53\delta\theta^3 + 56.818\delta\theta^2 - 5.5339\delta\theta + 31.107 \quad (31)$$

where $\delta\theta$ is in deg. and for $|\delta\theta| < 0.05$, t_d =0. With this strategy, an initial down-range deviation of $\pm$ 50 km can be handled. The reference trajectory for the simulations is obtained by open-loop integration of a selected reference control vector[22] $u_r = (\sigma_r, C_{L_r})^T$. Simulations were performed for a range of initial offsets from the reference trajectory and some of them are presented in this section. The weighting matrices (Q,R) are chosen by a similar procedure presented above for Model I. The altitude profile, ground-track, and the required control inputs are plotted in Fig. 5 for both positive (Case A) and negative perturbations (Case B) in longitude, latitude and altitude (Case I of Table 1) which is the largest perturbations reported in Ref. 22. The controlled trajectory follows the reference trajectory after a short period of time as shown in Fig. 5. In Ref. 22, a nonlinear control strategy is used for tracking the ground-track with a terminal error less than 1 n.m (1.85 km), with only one variable perturbed at a time. Our control strategy is able to track the ground-track more accurately without exceeding 1 km terminal error in ground-track (Fig. 6), with simultaneous perturbations in all state variables.. The difference in the perturbations and final ground-track error tolerance of Ref. 22 and the present method is highlighted in Table 5. The heating rate for the Model II is calculated using the empirical expression[25]

$$Q_h = 1.1969\text{x}10^4 \sqrt{\rho} V^{3.15} \quad (32)$$

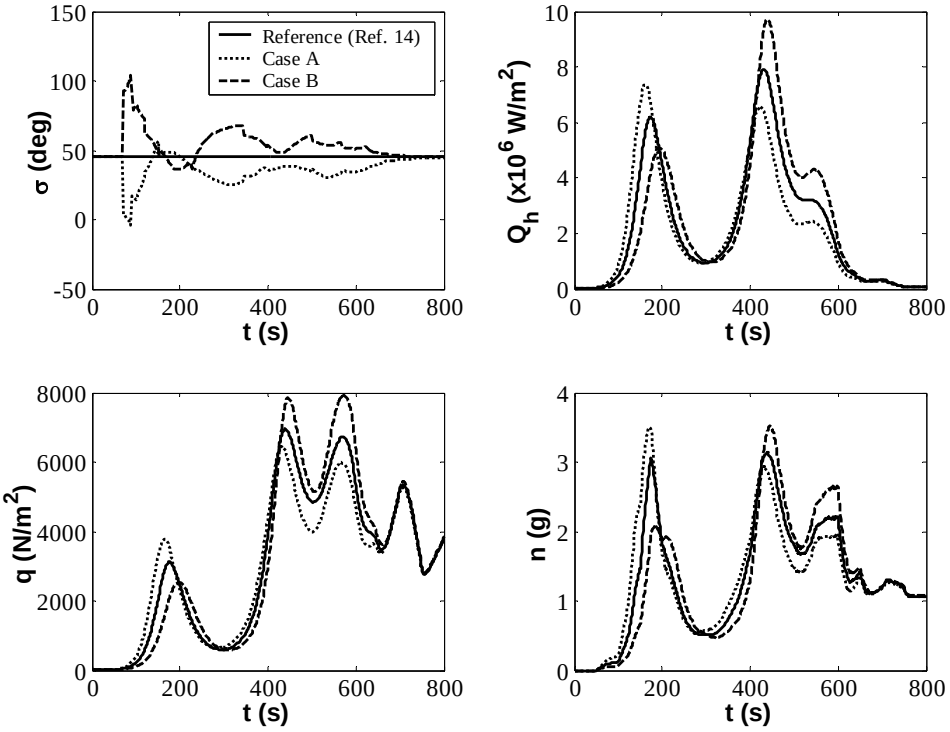

Figure 2. Control inputs and aero-thermal loads for Model I using Controller B

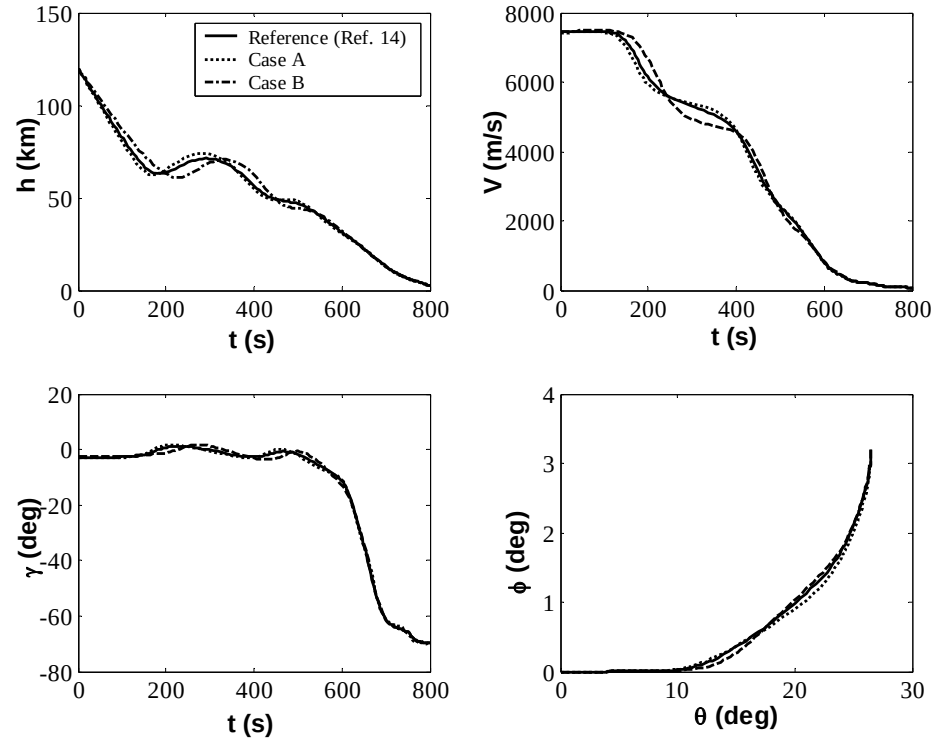

Figure 3. Trajectory profiles and ground-track for Model I using Controller A

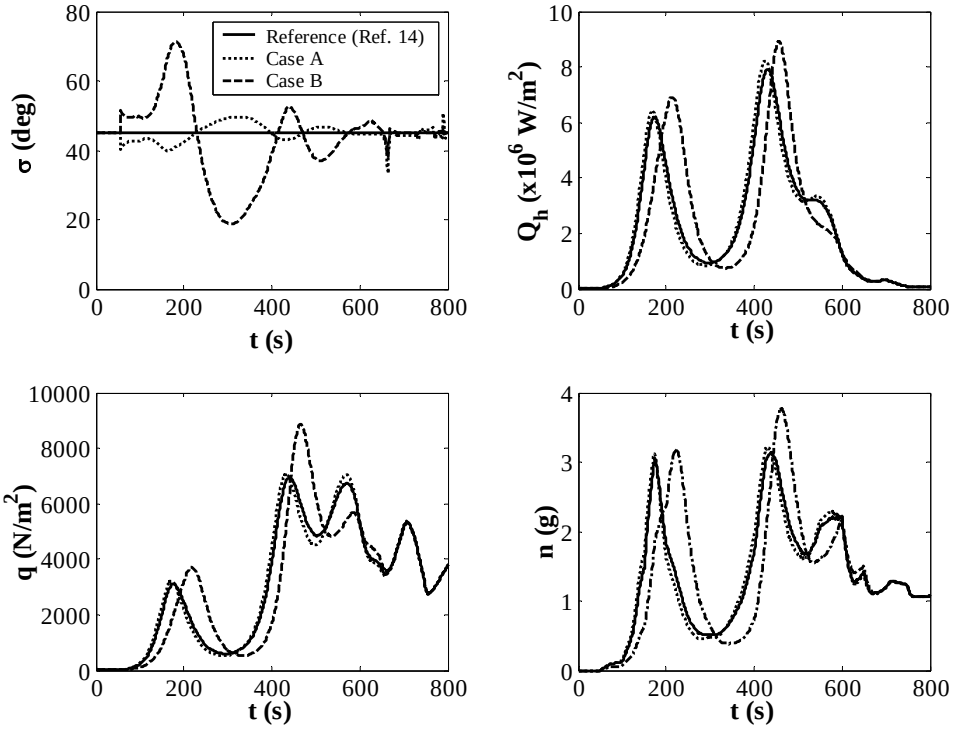

Figure 4. Control inputs and aero-thermal loads for Model I using Controller B

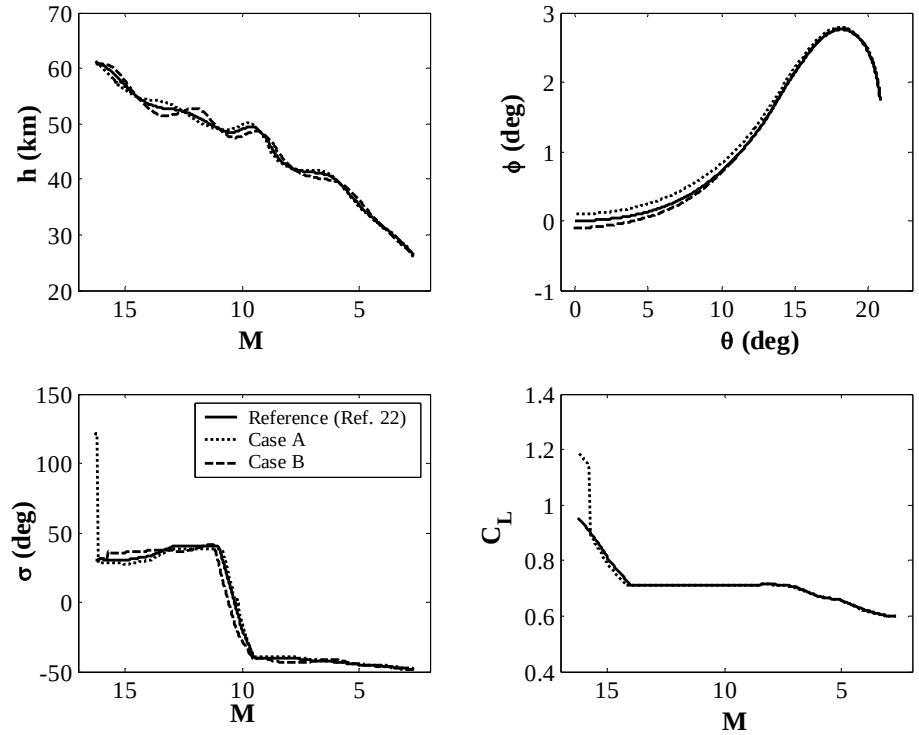

Figure 5. Altitude profile, ground-track and control inputs for Model II for Case I

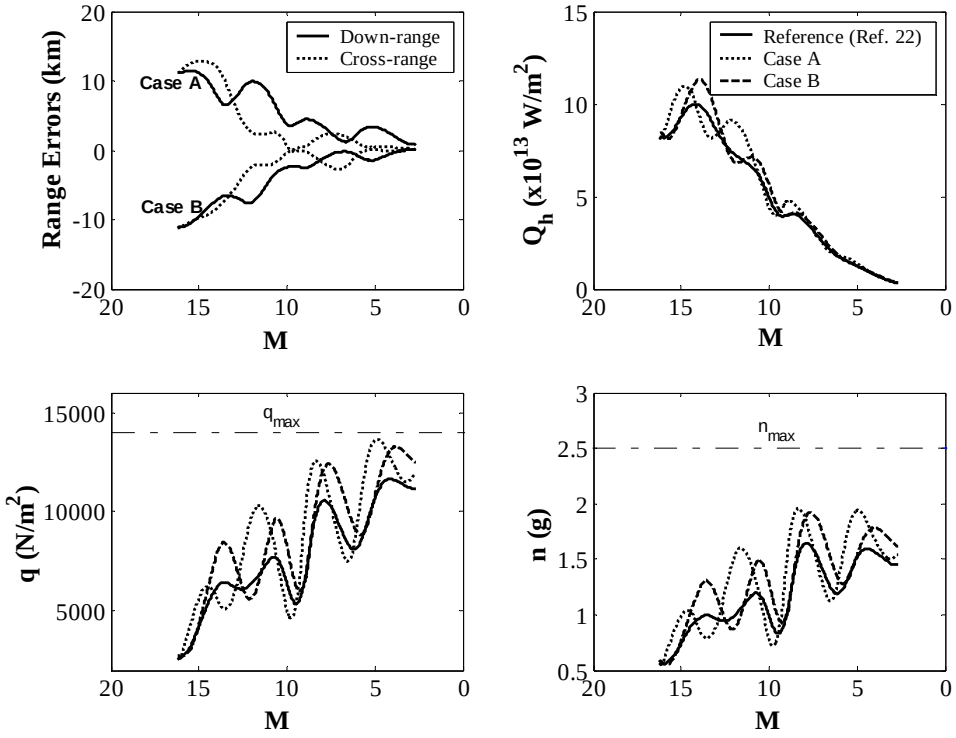

Figure 6. Range errors and aero-thermal loads for Model II for Case I

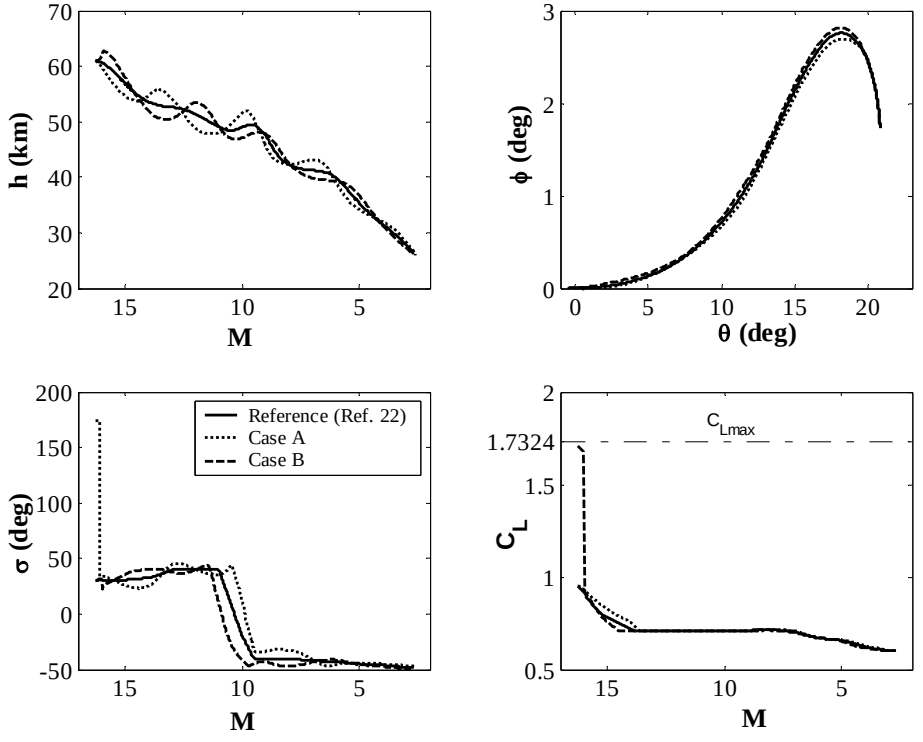

Figure 7. Altitude profile, ground-track and control inputs for Model II for Case II

Table 5. Comparison of range errors with Ref. 22 for Model II for Case I

Case	Description	Terminal ground track errors δR_c (km)
1	One state variable perturbed at a time (Ref. 22)	δR_c<1.85
2	All state variables perturbed simultaneously (present method)	δR_c<0.83

For both the cases
δx=[304.8 m, 0.1 deg., 0.1 deg., 30.48 m/s, 0.1 deg., 0.1 deg.]

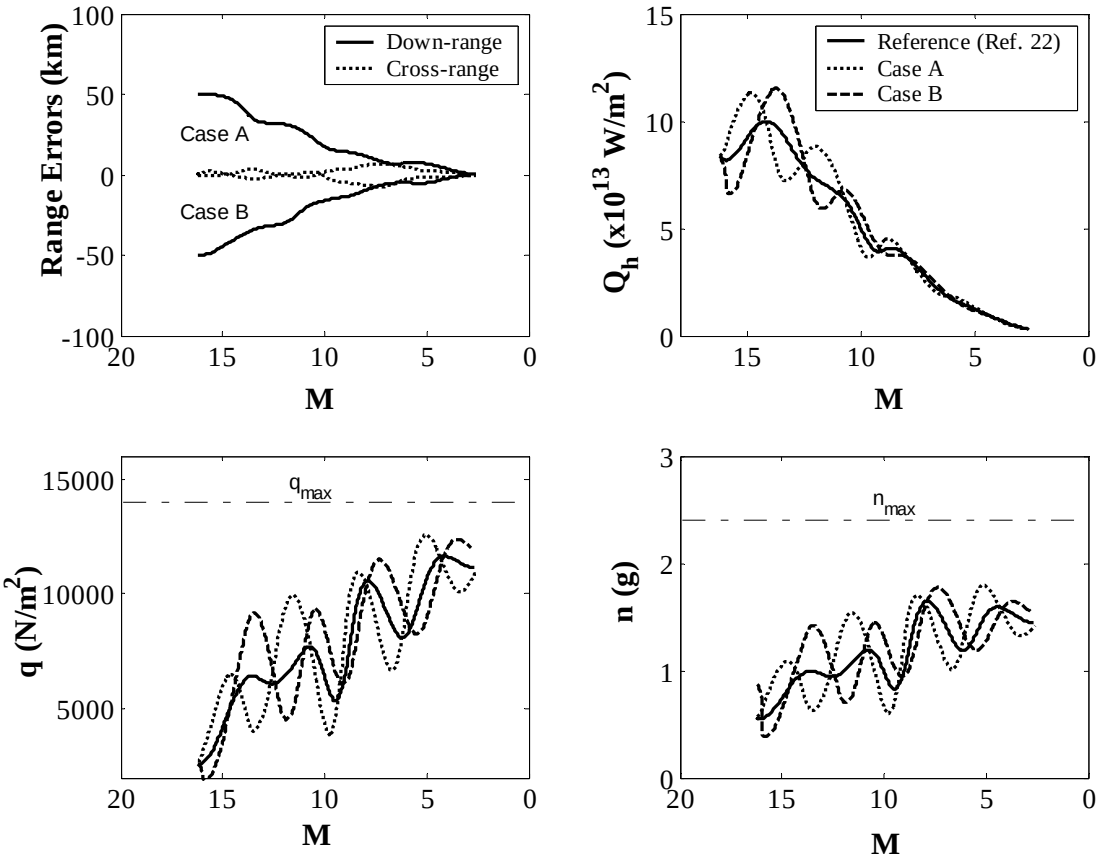

Figure 8. Range errors and aero-thermal loads for Model II for Case II

In Fig. 7, it is demonstrated that the present strategy performs well even in the presence of much larger deviations in the initial conditions (Case II of Table 1), than those previously reported[19, 22]. (In Ref. 19, a sliding mode control is used for $\delta X = \pm 28$ km, while Ref.22 considers $\delta X = \pm 11$ km; we reiterate that the present method can handle $\delta X = \pm 50$ km). Table 6 lists the required values of t_d for various down-range perturbations. This data is used for obtaining the empirical relations of Eqs. (30) and (31).

Table 6. Duration of smart maneuvering and ground-track errors for Model II for Case II

Case	Perturbation in longitude $\delta\theta$ (deg.)	Duration of smart maneuvering, t_d (s)	Terminal ground track errors δR_c (km)
1	+ 0.10	31.0	0.2420
2	+ 0.20	18.0	0.2361
3	+ 0.30	14.0	0.2927
4	+ 0.40	13.0	0.3531
5	+ 0.45	13.0	0.5879
6	- 0.10	32.0	0.1741
7	- 0.20	33.0	0.1446
8	- 0.30	33.5	0.2262
9	- 0.40	34.0	0.4134
10	- 0.45	34.5	0.4397

Table 7. Terminal state errors and maximum aero-thermal loads for Model II for +50 km deviation in down-range for full-state feedback and with Kalman filter

Errors at terminal time and maximum aero-thermal loads	Full-state feedback	With Kalman filter
δR_c (km)	0.5879	0.6242
δr (m)	0.2627	-1.2350
δV (m/s)	24.763	2.8008
$\delta\gamma$ (deg.)	1.3357	-2.7432
$\delta\psi$ (deg.)	0.08067	-9.5862
$Q_{h_{\max}}$ (W/m^2)	1.1316x10^{14}	1.1595x10^{14}
$q_{\max}$ (N/m^2)	1.2569x10^4	1.1177x10^4
$n_{\max}$ (g)	1.7958	1.7169

The necessary control inputs are plotted in Fig. 7, which shows that the upper limit on $C_{L_{\max}}$ is not exceeded, while the aero-thermal loads are plotted in Fig. 8, showing a slight increase in the peak loads, which are still within allowable limits.

A reduced-order linear Kalman filter is designed based upon the measurement of longitude, latitude and speed. Table 7 shows the terminal state errors and the maximum aero-thermal loads for the +50 km deviation in the down-range. It can be observed that the terminal errors increase slightly with Kalman filter, but remain quite small. Fig. 9 compares the altitude profile, ground-track, and control inputs of the full-state feedback with those of the Kalman filter. Fig. 10, demonstrates that the peak heating rate and maximum load-factor with Kalman filter are within the allowable limits.

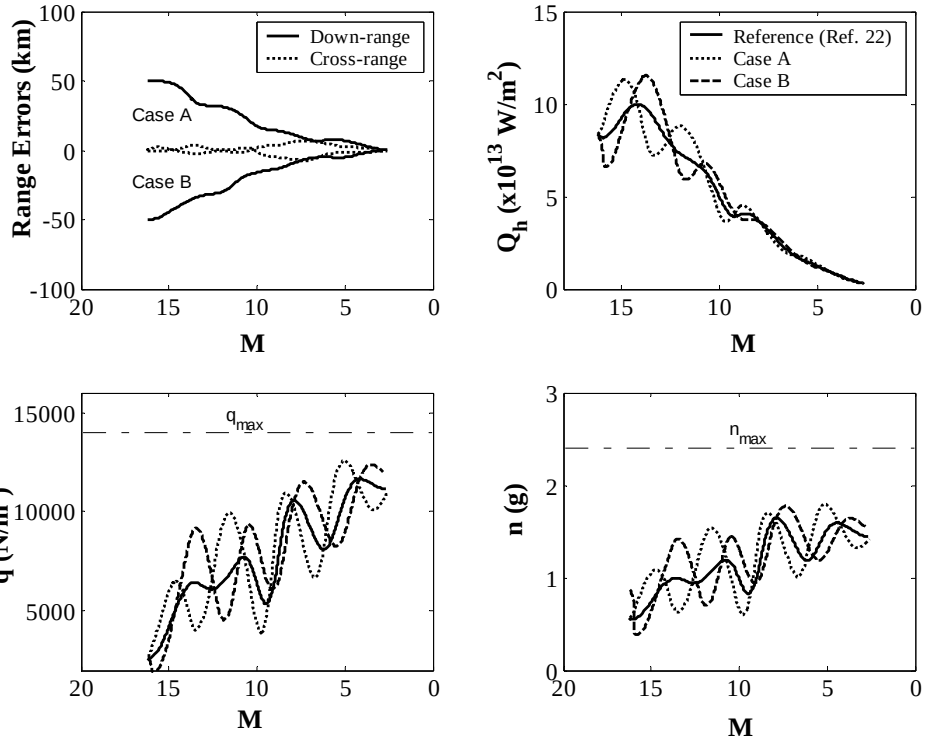

Figure 8. Range errors and aero-thermal loads for Model II for Case II

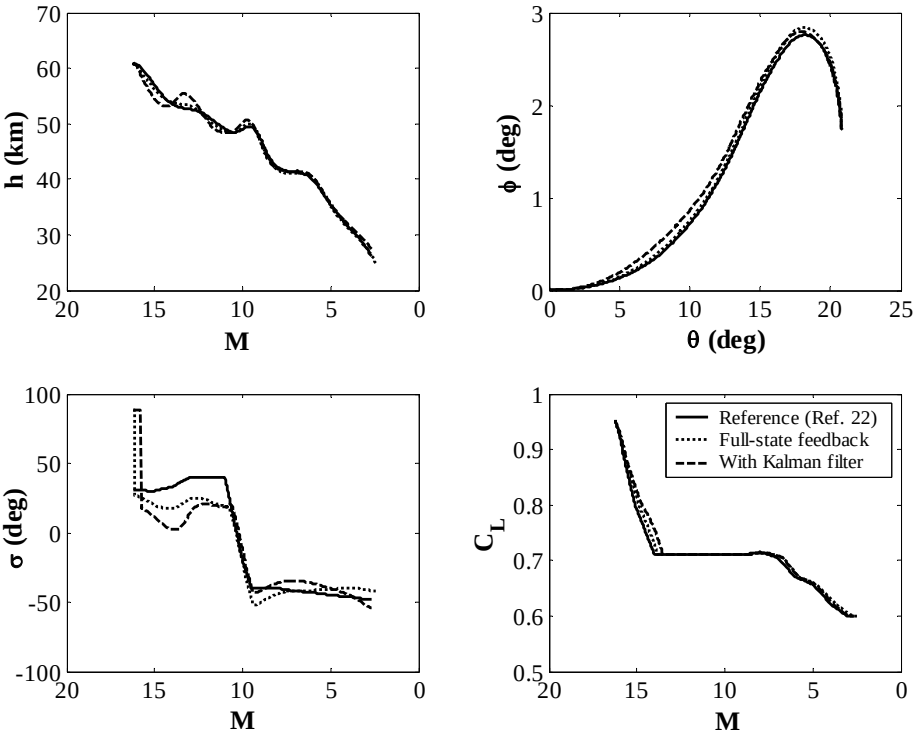

Figure 9. Altitude profile, ground-track and control inputs for Model II using Kalman filter

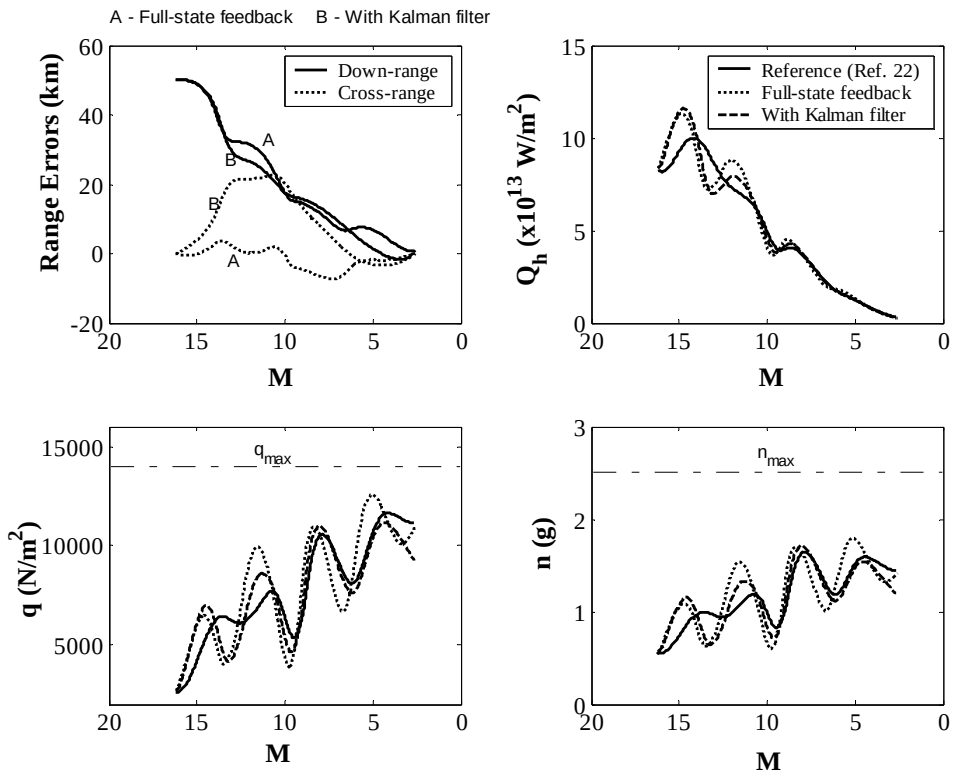

Figure 10. Range errors and aero-thermal loads for Model II using Kalman filter

V. Conclusion

The re-entry trajectory control using a combined strategy of down-range maneuvering and LQ optimal control has been applied to a low L/D payload vehicle as well as an RLV. The weighting matrices in the LQ technique are chosen such that the terminal state errors are small, and the aero-thermal loads acting on the vehicle are within allowable limits. The new strategy is shown to compensate for much larger deviations from a nominal RLV trajectory, when compared to a nonlinear tracking control derived using feedback linearization. Furthermore, it is shown that the LQ control has the advantage of good robustness when combined with a linear Kalman filter based upon the measurement of longitude, latitude and speed. Thus, it is demonstrated that a simple control concept is sufficiently accurate for re-entry trajectory control in the presence of moderate deviations in entry conditions, and can be directly implemented in actual entry vehicles.

References

[1]Wingrove, R.C., "Survey of Atmosphere Re-entry Guidance and Control Methods," *AIAA Journal*, Vol. 1, No. 9, Sept. 1963, pp. 2019-2029.

[2]Tannas Jr, L.E., "Re-entry guidance through closed-form equations," *AIAA Journal*, Vol. 5, No. 6, Jun. 1967, pp. 1102-1109.

[3]Shen, Y.C., "Series solution of equations for re-entry vehicles with variable lift and drag coefficients," *AIAA Journal*, Vol. 1, No. 11, Nov. 1963, pp. 2487-2490.

[4]Loh, W. H. T., *Dynamics and Thermodynamics of Planetary Entry*, Prentice-Hall Inc., Englewood Cliffs, N. J., 1963.

[5]Williamson, W. E., and Tapley, B. D., "Comparison of linear and Riccati equations used to solve optimal control problems," *AIAA Journal*, Vol.10, No. 9, Oct. 1972, pp. 1154-1159.

[6]Stoer, J., and Bulirsch, R., *Introduction to Numerical Analysis*, Springer-Verlag, 1980.

[7]Yeo, B. P., and Sng K. B., "Numerical solution of the constrained re-entry vehicle trajectory problem via quasilinearization," *Journal of Guidance, Control, and Dynamics*, Vol. 3, No. 5, 1980, pp. 392–397.

[8]Trent, A., Venkataraman, R., and Doman, D., "Trajectory generation using a modified simple shooting method," (2004), *Proc. IEEE Aerospace conference*, Big Sky, MT.

[9]Harpold, J. C., and Graves, C. A., “Shuttle Entry Guidance,” *Journal of the Astronautical Sciences*, Vol. 37, No. 3, 1979, pp. 239–268.

[10]Harpold, J. C., and Gavert, D. E., “Space Shuttle Entry Guidance Performance Results,” *Journal of Guidance, Control, and Dynamics*, Vol. 6, No. 6, 1983, pp. 442–447.

[11]deVirgilio, M.A., Wells, G.R., and Schiring, E.E., "Optimal Guidance for Aerodynamically Controlled Re-Entry Vehicles," *AIAA Journal*, Vol.12, No. 10, Oct. 1974, pp. 1331-1337.

[12]Sworder, D.D. and Wells, G.R., “Guidance Laws for Aerodynamically Controlled Re-Entry Vehicles,” *Journal of Spacecraft and Rockets*, Vol. 14, Feb. 1977, pp. 111-117.

[13] Archer, S. M., “Selection of Guidance Variable for a Re-entry Vehicle,” *Journal of Guidance, Control, and Dynamics*, Vol. 2, No. 2, 1979, pp. 130–138.

[14]Roenneke, A. J., and Cornwell, P. J., “Trajectory Control for a Low-Lift Re-Entry Vehicle,” *Journal of Guidance, Control, and Dynamics*, Vol. 16, No. 5, 1993, pp. 927–933.

[15]Roenneke, A. J., and Markl, A., “Reentry Control to a Drag-vs-Energy Profile,” *Journal of Guidance, Control, and Dynamics*, Vol. 17, No. 5, 1994, pp. 916–920.

[16]Lu, P., "Regulation about Time-Varying Trajectories: Precision Entry Guidance Illustrated," *Journal of Guidance, Control, and Dynamics*, Vol. 22, No. 6, 1999, pp. 784-790.

[17]Shen, Z., and Lu, P., "Dynamic Lateral Entry Guidance Logic," *Journal of Guidance, Control, and Dynamics*, Vol. 27, No. 6, 2004, pp. 949-959.

[18]Mease, K. D., and Kremer, J. P., “Shuttle Entry Guidance Revisited Using Nonlinear Geometric Methods,” *Journal of Guidance, Control, and Dynamics*, Vol. 17, No. 6, 1994, pp. 1350–1356.

[19]Cavallo, A., and Ferrara, F., “Atmospheric Re-entry Control for Low Lift/Drag Vehicles,” *Journal of Guidance, Control, and Dynamics*, Vol. 19, No. 1, 1996, pp. 47–53.

[20]Lu, P., “Entry Guidance and Trajectory Control for Reusable Launch Vehicle,” *Journal of Guidance, Control, and Dynamics*, Vol. 20, No. 1, 1997, pp. 143–149.

[21]Lu, P., and Hanson, J.M., “Entry Guidance for the X-33 Vehicle,” *Journal of Spacecraft and Rockets*, Vol. 35, No. 3, 1998, pp. 342–349.

[22]Bharadwaj, S., Rao, A. V., and Mease, K. D., “Entry Trajectory Tracking Law via Feedback Linearization,” *Journal of Guidance, Control, and Dynamics*, Vol. 21, No. 5, 1998, pp. 726–732.

[23]Vinh, N. X., “Equations of Motion,” *Flight Mechanics of High Performance Aircraft*, Cambridge Aerospace Series 4, Cambridge Univ. Press, New York, 1993.

[24]Tewari, A., *Modern control design with MATLAB and SIMULINK*, Wiley, Chichester, U.K., 2002.

[25]Shen, Z., and Lu, P., "Onboard generation of three-dimensional constrained entry trajectories," *Journal of Guidance, Control, and Dynamics*, Vol. 26, No. 1, 2003, pp. 111-121.